

www.acsami.org Research Article

# Effect of Europium and Gadolinium Alloying Elements on the Tribological Response of Low Hydrogen Content Amorphous Carbon

Camille Edwards, Hsu-Ming Lien, Nicolás Molina, and Filippo Mangolini\*



Cite This: https://doi.org/10.1021/acsami.4c00677



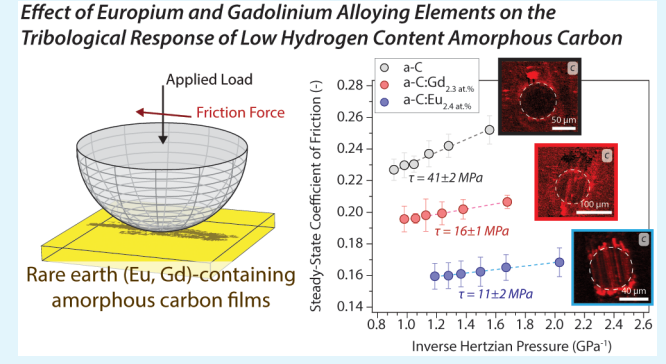
ACCESS

Metrics & More

Article Recommendations

Supporting Information

ABSTRACT: Dopants and alloying elements are commonly introduced in amorphous carbon (a-C) materials to tailor their mechanical and tribological properties. While most published studies have focused on doping and alloying a-C coatings with metals or metalloids, doping a-C films with rare-earth elements has only recently been explored. Notably, our understanding of the shear-induced structural changes occurring in rare-earth-element-containing a-C films is still elusive, even in the absence of any liquid lubricants. Here, the friction response of Eu- and Gd-containing a-C films with low hydrogen content deposited by HiPIMS on silicon was evaluated in open air and at room temperature. The load-dependent friction measurements indicated that the introduction of Gd ((2.3  $\pm$  0.1) at.%) and Eu ((2.4  $\pm$  0.1)



at.%) into the a-C matrix results in a significant reduction of the shear strength of the sliding interfaces ((41  $\pm$  2) MPa for a-C, (16  $\pm$  1) MPa for a-C:Gd<sub>2.3 at.%</sub>, and (11  $\pm$  2) MPa for a-C:Eu<sub>2.4 at.%</sub>). NEXAFS spectromicroscopy experiments provided evidence that no stress-assisted sp<sup>3</sup>-to-sp<sup>2</sup> rehybridization of carbon atoms was induced by the sliding process in the near-surface region of undoped a-C, while the amount of sp<sup>2</sup>-bonded carbon progressively increased in a-C:Gd<sub>2.3 at.%</sub> and a-C:Eu<sub>2.4 at.%</sub> upon increasing the applied normal load in tribological tests. The formation of an sp<sup>2</sup>-bonded carbon-rich surface layer in a-C:Gd<sub>2.3 at.%</sub> and a-C:Eu<sub>2.4 at.%</sub> films was not only proposed to be the origin for the reduced duration of the running-in period in tribological test, but was also postulated to induce shear localization within the sp<sup>2</sup>-carbon-rich layer and transfer film formation on the countersurface, thus decreasing the interfacial shear strength. These findings open the path for the use of Gd- and Eu-containing a-C even under critical conditions for nearly hydrogen-free a-C films (i.e., humid air).

KEYWORDS: diamond-like carbon, alloyed DLC, NEXAFS, amorphous carbon, spectromicroscopy, tribology

# 1. INTRODUCTION

Amorphous carbon-based (a-C) materials, also referred to as diamond-like carbons (DLCs), have attracted considerable scientific and technological interest in the last decades owing to their unique mechanical properties (e.g., high strength, high wear resistance, low adhesion, and low friction). 1,2 This has resulted in their use in a variety of applications, including as solid lubricating coatings for automotive<sup>3</sup> and aerospace<sup>4</sup> components, coatings for machining tools, overcoat films for hard disks,6 and even as thin films on high-aspect-ratio features, such as atomic force microscope (AFM) probes. Although DLCs have been employed with success in several sectors, their wider use has been constrained by critical challenges. For example, hydrogenated amorphous carbon (a-C:H) films, which contain a significant fraction of hydrogen and sp<sup>2</sup>-hybridized carbon atoms, exhibit limited thermal stability as they rapidly degrade at temperatures above 150  $^{\circ}$ C<sup>8,9</sup> and show an increase in friction with increasing relative humidity,  $^{1,4,10,11}$  which is attributed to the surface adsorption of oxygen and/or water. <sup>10,11</sup> As another example, tetrahedral amorphous carbon (ta-C) films, which contain a high fraction of sp³-bonded carbon atoms and are hydrogen-free ([H] < 5 at. %), <sup>12</sup> show a high friction and wear response in vacuum and dry environments¹ as a result of the generation of strong C–C covalent bonds at the sliding interface following the removal of passivating species. <sup>1,2</sup> While a reduction of friction and wear for ta-C was reported to occur upon introducing gaseous species in the environment that can dissociatively adsorb on the ta-C surface and saturate dangling bonds, <sup>13–30</sup> the friction response in ambient conditions is still significantly higher than

Received: January 12, 2024 Revised: April 23, 2024 Accepted: May 8, 2024



the response of a-C:H in dry or vacuum conditions. Notably, molecular dynamics (MD) simulations combined with nearedge X-ray absorption fine structure (NEXAFS) spectroscopy analyses provided further insights into the phenomena occurring at ta-C/ta-C sliding interfaces<sup>31</sup> and demonstrated that surface passivation is not the only physicochemical process taking place in the presence of reactive gas species (e.g., water molecules): The removal of passivating species at colliding nanoscale asperities leads to the stress-induced formation of an amorphous carbon (a-C) layer with a higher fraction of carbon atoms in sp<sup>2</sup> hybridization. As sliding proceeds, shear localization occurs within the a-C layer, and surface passivation (through the dissociative reaction of gaseous species) takes place once asperities separate.

To overcome the shortcomings of a-C:H and ta-C materials, deposition processing methods have been modified to introduce dopants and alloying elements into the a-C matrix. 9,32 For example, coatings made of hydrogenated amorphous carbon containing silicon and oxygen have attracted considerable attention owing to their low residual stress (typically <1 GPa),<sup>33</sup> higher thermal<sup>34–37</sup> and thermooxidative<sup>38</sup> stability than undoped a-C:H, as well as low friction and wear response across a broader range of conditions and environments in comparison to a-C:H and ta-C films.<sup>33</sup> Recently, Mangolini et al. evaluated the tribological response of hydrogenated amorphous carbon ([H] =  $(34 \pm 1)$  at.%)) containing silicon and oxygen ([Si] =  $(6 \pm 1)$  at.%; [O] =  $(3 \pm 1)$ 1) at.%) sliding against steel under different environmental conditions, from high vacuum to high hydrogen and oxygen gas pressure.<sup>39,40</sup> The correlation of the friction and wear results with the outcomes of imaging NEXAFS measurements indicated that the tribological behavior of the coating is influenced by its gas-pressure-dependent surface termination. While surface termination was strongly dependent on the nature of the gaseous environments (i.e., hydrogen vs oxygen) in which the sliding experiments were performed, the NEXAFS data also demonstrated the stress-induced sp<sup>3</sup>-to-sp<sup>2</sup> rehybridization of carbon atoms in the near-surface region.

While most published studies focused on doping and/or alloying a-C coatings with metals or metalloids,<sup>32</sup> doping a-C films with rare-earth elements<sup>41–45</sup> and rare-earth oxides<sup>46,47</sup> has only recently been explored. As one example, Omiya et al., 42 Sadeghi et al., 45 and Shaikh et al. 41 evaluated the tribological properties of gadolinium (Gd)- and europium (Eu)-alloyed a-C films deposited by high power impulse magnetron sputtering (HiPIMS) in the presence of synthetic oil containing a class of promising additives for transmission fluids, namely phosphonium phosphate ionic liquids. 48,49 The results of tribological experiments and scanning electron microscopy-energy dispersive spectroscopy (SEM-EDS) measurements indicated that only the introduction of Gd in the a-C matrix favors the formation of a transfer layer on the steel counterbody that enhances the generation and adhesion of a lubricious and antiwear boundary layer (i.e., tribofilm) from the lubricant additives.<sup>42</sup> As another example, Meng et al. investigated the effect of the introduction of lanthanum (La) in DLC films grown by magnetron sputtering on the resulting mechanical, tribological, and wetting properties.44 The experimental results indicated that the presence of small amounts of La (≈7 at. %) in DLC lowers the residual stress in the coating, while reducing the film hardness and elastic modulus. Notably, the authors also indicated that La atoms catalyze the generation and ordering of sp<sup>2</sup>-bonded carbon.

Despite the relevance of these studies, our understanding of the shear-induced structural changes occurring in Eu- and Gd-containing a-C films is still elusive, particularly in the absence of any liquid lubricants. The present work aims to fill this knowledge gap by evaluating the normal-pressure-dependent friction response of Eu- and Gd-containing a-C films and correlating it with the changes occurring in the near-surface region of the coatings by performing NEXAFS spectromicroscopy measurements.

#### 2. MATERIALS AND METHODS

2.1. Deposition of Eu- and Gd-Containing DLC Coatings. The deposition of Eu- and Gd-containing a-C coatings was performed by high-power impulse magnetron sputtering (HiPIMS) using a deep oscillation magnetron sputtering (DOMS) power supply (HiPIMS Cyprium plasma generator, Zpulser Inc.), as recently described in ref 42. Briefly, the deposition chamber is equipped with a pure graphite target (99.95%) as well as a chromium target, which was used to deposit an adhesion layer. The graphite target was employed to grow pure a-C films. To obtain Eu- and Gd-containing a-C films, circular Gd and Eu pellets (diameter: 10 mm; depth: 2 mm) were glued onto the graphite target. The number of pellets was varied to systematically fine-tune the concentration of Eu and Gd in the films. During the deposition process, the substrate and target were maintained at a distance of ≈80 mm. The growth procedure included three steps: (i) substrate and target etching with argon, (ii) deposition of an adhesion interlayer (≈400 nm thick), and (iii) growth of the a-C films. In this study, a-C coatings with an Eu and Gd content of, respectively,  $(2.4 \pm 0.1)$  at.% and  $(2.3 \pm 0.1)$  at.% (determined by Rutherford backscattering spectrometry (RBS)) and a thickness of  $(1.7 \pm 0.1) \mu m$  were grown on silicon wafers. The hydrogen content in the films (determined by Rutherford backscattering spectrometry (RBS) and elastic recoil detection (ERD)) was found to be extremely low (between 3 and 6 at. %, with an uncertainty of  $\pm 3$  at. % for the hydrogen concentration from RBS/ERD measurements).

**2.2. Methods.** Reciprocating ball-on-flat experiments were performed by using a Bruker UMT TriboLab (Bruker, USA). The flat silicon substrates ( $10 \times 10$  mm) were coated with Euor Gd-containing a-C films, while the spherical countersurfaces (diameter: 4 mm) were made of 52100 steel. The applied normal load was varied between 1 N (average contact pressure as low as 0.49 GPa) and 5 N (average contact pressure as high as 1.3 GPa), while the stroke length and sliding speed were 2 mm and 1 mm s<sup>-1</sup>, respectively. All tests were carried out in open air (relative humidity: 35-55%) at room temperature (( $22 \pm 3$ ) °C). At the end of sliding experiments, the samples were stored in desiccators before being analyzed.

Nanoindentation measurements were performed in air and at room temperature using a Hysitron Triboindenter TI 950 instrument (Hysitron, Bruker, USA). The indenter was operated in a load-controlled indentation mode with partial cycling (up to 8 mN, initial force of 20  $\mu$ N) to assess the indepth mechanical properties of the films. Fused silica samples were used before each set of experiments to ensure that the shape factor of the Berkovich diamond indenter was properly calibrated. The reduced elastic modulus ( $E^*$ ) and hardness (H) were calculated using the Oliver–Pharr method. <sup>50</sup>

Near-edge X-ray absorption fine structure (NEXAFS) spectromicroscopy measurements were performed at the National Synchrotron Light Source II (NSLS-II, Brookhaven

National Laboratory, USA) at beamline 7-ID-1 (SST-1). The full-field spectromicroscope (known as the Large Area Rapid Imaging Analytical Tool, LARIAT, Synchrotron Research Inc., Melbourne Beach, FL, USA) allows for the acquisition of X-ray absorption imaging data with a 13 mm × 18 mm field of view and a lateral resolution of  $\approx 50 \ \mu \text{m}$ . In the present work, carbon K-edge NEXAFS data were acquired in partial electron yield (PEY) mode at a photon energy between 270 and 330 eV. NEXAFS image stacks were processed using LDF software (Synchrotron Research Inc., Melbourne Beach, FL, USA). The processing procedure included normalization of NEXAFS data to the drain current simultaneously measured by a clean Aucoated mesh upstream of the endstation, followed by normalization to the pre-edge spectral intensity. To ensure that variations in spectral intensity are only caused by changes in carbon bonding environment and are not dependent on the number density of absorbing atoms, a post-edge intensity normalization was finally performed.

The quantification of the fraction of sp²-bonded carbon ( $f_{\rm sp}$ ²-bonded carbon ( $f_{\rm sp}$ ²-bonded out following the procedure described in refs 53 and 54, which relies on the areas of the C 1s  $\rightarrow$   $\pi$ \* and C 1s  $\rightarrow$   $\sigma$ \* signals for the sample under investigation and a reference sample:

$$f_{\rm sp^2} = \frac{I_{\rm sample}^{\pi^*}}{I_{\rm sample}(\Delta E)} \frac{I_{\rm ref}(\Delta E)}{I_{\rm ref}^{\pi^*}} \tag{1}$$

where  $I_{\rm sample}^{\pi^*}$  and  $I_{\rm ref}^{\pi^*}$  are the areas of the C 1s  $\to \pi^*$  peaks for, respectively, the sample and the reference, while  $I_{\rm sample}(\Delta E)$  and  $I_{\rm ref}(\Delta E)$  are the integrated intensity (between 288.6 and 320 eV) for, respectively, the sample and the reference. In the present work, reference carbon K-edge spectra were collected on freshly cleaved highly ordered pyrolytic graphite (HOPG, grade 2, SPI Supplies, West Chester, PA, USA) (100% sp²-bonded carbon) following the procedure described in refs 53, 54, and 55.

Scanning electron microscopy (SEM) and energy-dispersive spectroscopy (EDS) analyses were carried out with a Tescan Vega 3 microscope (Tescan, Czech Republic) equipped with a Bruker EDS XFlash detector 630 M (Bruker, USA). EDS element mapping was acquired at a working distance of 15 mm and with a beam energy of 2.5 kV.

The surface composition of the coatings was determined by X-ray photoelectron spectroscopy (XPS). XPS analyses were performed using a VersaProbe IV XPS instrument (ULVAC-PHI, USA) operating at a base pressure below  $1 \times 10^{-9}$  Torr. The spectrometer was calibrated following the ISO 15472:2001 standard with an accuracy of  $\pm 0.1$  eV. Spectra were acquired using a monochromatized Al Ka X-ray source with an X-ray beam of 100  $\mu$ m at three different emission angles  $(0^{\circ}, 45^{\circ}, \text{ and } 60^{\circ})$ . Survey spectra were collected with a pass energy of 140 eV, while high-resolution spectra were acquired with a pass energy of 27 eV and a step size of 0.1 eV (full-width-at-half-maximum (fwhm) of the Ag  $3d_{5/2}$  peak equal to 0.55 eV). Data processing was carried out using CasaXPS (version 2.3.25, Casa Software Ltd., UK) and included background subtraction (performed using an iterated Shirley-Sherwood algorithm) prior to peak fitting. Quantitative analysis of the surface composition was performed using the method described in refs 56 and 57.

#### 3. RESULTS AND DISCUSSION

Nanoindentation measurements were performed to evaluate the depth dependence of the mechanical properties of asdeposited Eu- and Gd-containing a-C films. Figure 1a,c

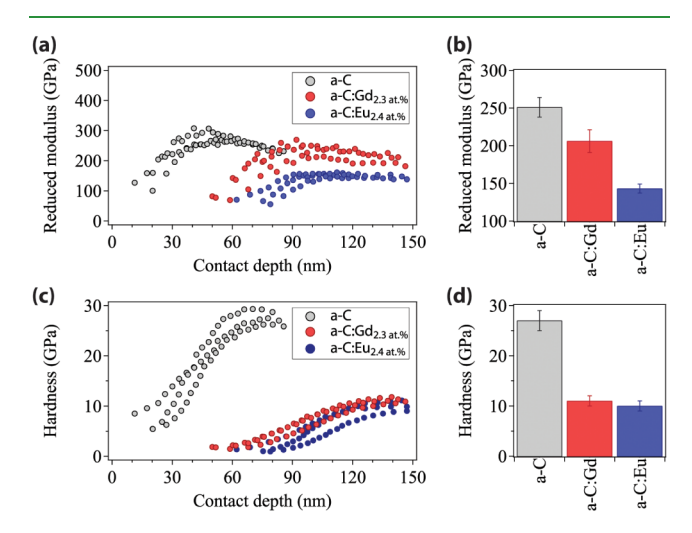


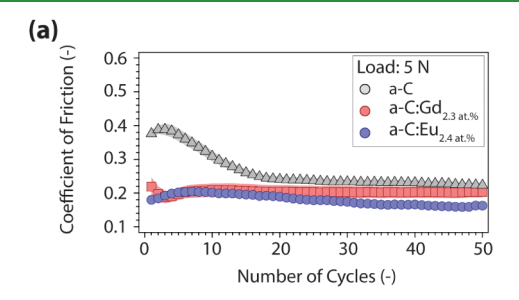
**Figure 1.** (a) Reduced elastic modulus and (c) hardness as a function of depth for as-deposited a-C, a-C:Gd $_{2.3}$  at $_{90}$ , and a-C:Eu $_{2.4}$  at $_{90}$  films. The average reduced elastic moduli and hardness computed considering an indentation depth range that allows for mitigating potential artifacts originating from surface roughness and substrate effects are displayed in (b) and (d).

respectively show the reduced elastic modulus  $(E^*)$  and hardness (H) as a function of depth from the sample surface, where the first measured contact depth for the initial load of 20  $\mu$ N is 11 nm for a-C, 50 nm for a-C:Gd<sub>2.3 at.%</sub>, and 62 nm for a-C:Eu<sub>2.4 at.%</sub>. Figure 1b,d display the average values of  $E^*$  and Hcomputed considering an indentation depth range (between 60 and 90 nm for a-C films and between 125 and 150 nm for Euand Gd-containing a-C films) that allows for mitigating potential artifacts originating from surface roughness (note: the average roughness was between 2 and 4 nm for the asdeposited coatings as measured by AFM over a 2  $\mu$ m  $\times$  2  $\mu$ m area) and substrate effects. Assuming a Poisson's ratio of 0.2 for the a-C films<sup>58</sup> as well as an elastic modulus and a Poisson's ratio of, respectively, 1141 GPa and 0.07 for the indenter, 59 the elastic moduli were (308  $\pm$  13) GPa for a-C, (241  $\pm$  15) GPa for a-C:Gd<sub>2.3 at%</sub>, and (143  $\pm$  6) GPa for a-C:Eu<sub>2.4 at.%</sub>. Notably, the elastic modulus and hardness values for undoped a-C agree well with the values reported by Ohtake et al. for undoped DLC films grown using physical vapor deposition (PVD) processes. 12 The introduction of Eu and Gd in the a-C matrix did not only result in a significant decrease in both elastic modulus (-22% for a-C:Gd<sub>2.3 at.%</sub> and -49% for a-C:Eu<sub>2.4 at.%</sub>) and hardness (-59% for a-C:Gd<sub>2.3 at.%</sub> and -63%for a-C:Eu<sub>2.4 at.%</sub>) relative to undoped a-C, but also lead to the presence of an extended near-surface layer with reduced nanomechanical properties. The decrease in nanomechanical properties of DLC upon alloying it with Eu and Gd is in agreement with the results reported by Meng et al.,44 which indicated a reduction in DLC hardness ( $\sim -19\%$ ) and elastic modulus ( $\sim -20\%$ ) upon introducing small amounts of La  $(\approx 7 \text{ at. }\%)$  into the a-C matrix.

The origin for the extended near-surface layer with reduced nanomechanical properties in a-C:Eu<sub>2.4 at.%</sub> and a-C:Gd<sub>2.3</sub> is attributed to the surface enrichment in alloying elements in the

coatings since, as indicated by X-ray photoelectron spectroscopy (XPS) analyses (see XPS high-resolution spectra in Figure S1), the outermost region of the coatings is enriched in alloying elements ([C]/[Eu] = 14.4 in a-C:Eu<sub>2.4 at.%</sub> and [C]/[Gd] = 14.1 in a-C:Gd<sub>2.3</sub> from XPS data acquired at an emission angle of 45°) compared to the bulk of the films ([C]/[Eu] = 39.4 in a-C:Eu<sub>2.4 at.%</sub> and [C]/[Gd] = 39.9 in a-C:Gd<sub>2.3</sub> as determined by Rutherford backscattering spectrometry—a bulk-sensitive technique). This finding agrees well with the progressive reduction in nanomechanical properties of rare-earth-containing a-C films with the content of the alloying element recently reported by Tillmann et al.  $^{60}$ 

Reciprocating ball-on-flat (52100 steel balls-on-silicon wafers coated with a-C films) experiments were performed in open air (relative humidity: 35–55%) at room temperature ((22  $\pm$  3)  $^{\circ}$ C) at different applied normal loads (from 1 to 5 N). Figure 2a displays an example of the evolution of the



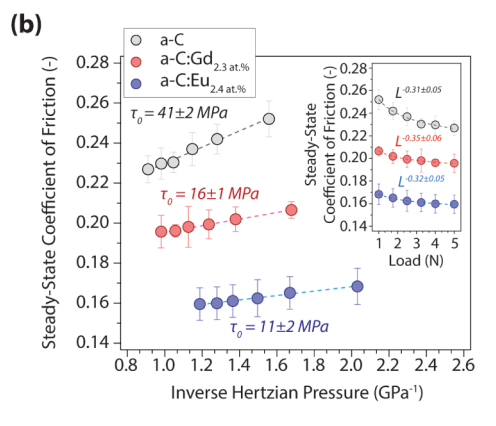


Figure 2. (a) Coefficient of friction as a function of sliding cycles measured during reciprocating ball-on-flat tests carried out in open air (relative humidity: 35–55%) at room temperature ((22  $\pm$  3)  $^{\circ}\text{C}$ ) using silicon wafers coated with a-C films (flat) and 52100 steel counterparts (spheres). (b) Steady-state coefficient of friction (computed considering the last 20 cycles) as a function of the inverse Hertzian contact pressure. The linear regression of the experimental data using eq 3 allowed for the computation of the interfacial shear strength  $(\tau_0)$  for the three coatings. The inset of (b) displays the variation of the steady-state coefficient of friction with the applied normal load (L). The steady-state CoF values shown in the inset were fitted using eq 2, thus allowing for the computation of the power-law coefficient (n).

coefficient of friction (CoF) as a function of sliding cycles for a-C, a-C:Gd<sub>2.3 at.%</sub>, and a-C:Eu<sub>2.4 at.%</sub> films under an applied normal load of 5 N. While in the case of a-C a distinct running-in period was observed and a steady-state friction response was only achieved after  $\approx\!20$  sliding cycles, in the case of a-C films containing either Gd or Eu a steady-state response was achieved after a short running-in (less than 10 cycles). The difference in running-in behavior between the undoped and

doped a-C films can be ascribed to the initial roughness of the contacting surfaces, which results in an increase in friction until surface smoothening and conformity take place. Owing to the higher mechanical properties of the a-C film compared to the ones of the doped a-C coatings, the initial transient in friction is enhanced in the former. It is worth noticing that the CoF of steel sliding against a-C in open air is in agreement with previously published reports under similar contact conditions. Notably, the steady-state CoF for Eu- and Gd-containing a-C films was always lower than the one measured in the experiments carried out with undoped a-C films.

Load-dependent friction measurements were performed to evaluate changes in interfacial shear strength induced by the introduction of Eu or Gd into the a-C matrix. The inset of Figure 2b displays the variation of the steady-state CoF with the applied normal load. As already reported for other solid lubricant coatings (e.g., DLCs, molybdenum disulfide, tungsten disulfide),  $^{33,63-66}$  a non-Amontonian friction behavior, i.e., a decrease in the CoF with the normal load, was observed for a-C, a-C:Gd2.3 at.%, and a-C:Eu2.4 at.% films. This behavior can be explained considering the Hertzian model for an elastic sphere-on-flat contact,  $^{67}$  according to which the friction coefficient has a power-law dependence on the applied load ( $\mu \propto L^{-1/3}$ , eq 2):

$$\mu = \tau_0 \pi \left(\frac{3R}{4E^*}\right)^{2/3} L^{-\frac{1}{3}} + \alpha \tag{2}$$

where  $\tau_0$  is the interfacial shear strength, R the sphere radius,  $E^*$  the reduced elastic modulus, and  $\alpha$  the pressure-dependent coefficient of the shear strength. To compute the normal load dependence of the CoF for the films deposited in the present study, the steady-state CoF values shown in the inset of Figure 2b were fitted using a power-law equation ( $\mu \propto L^{-n}$ ). In all cases, the power-law coefficient ( $n_{a\text{-}C}=0.31\pm0.05;\ n_{a\text{-}C\text{-}Gd}=0.35\pm0.06;\ n_{a\text{-}C\text{-}Eu}=0.32\pm0.05$ ) was in excellent agreement with the one appearing in the elastic contact model (n=1/3), thus indicating that the Hertzian contact behavior accurately describes the load-dependent friction response for a-C, a-C:Gd<sub>2,3 at,%</sub>, and a-C:Eu<sub>2,4 at,%</sub> films.

Performing sliding experiments at different normal loads also allows for the evaluation of the interfacial shear strength  $(\tau_0)$  since the CoF is inversely proportional to the average Hertzian contact pressure  $(P_{\rm mean})$ :  $^{33,63-66}$ 

$$\mu = \frac{\tau_0}{P_{\text{mean}}} + \alpha \tag{3}$$

Figure 2b displays the steady-state CoF as a function of the inverse Hertzian pressure for the case of experiments carried out with a-C, a-C:Gd $_{2.3~at,\%}$ , and a-C:Eu $_{2.4~at,\%}$  films. The linear regression of the experimental data allowed for the computation of the interfacial shear strength for the three coatings, which was found to be  $(41 \pm 2)$  MPa for a-C,  $(16 \pm$ 1) MPa for a-C:Gd<sub>2.3 at.%</sub>, and (11  $\pm$  2) MPa for a-C:Eu<sub>2.4 at.%</sub> (the values of the fitting parameters, i.e.,  $\tau_0$  and  $\alpha$ , are also reported in Table S1). The interfacial shear strength for a-C films sliding against steel is in agreement with previously reported values for DLC/sapphire (38 MPa) and DLC/steel (36 MPa) contacts sliding in open air<sup>65</sup> as well as diamond/ diamond contacts sliding in water vapor (31-47 MPa) and hydrogen gas (11-39 MPa).<sup>25</sup> It is worth noticing that the interfacial shear strength for a-C films sliding against steel computed in the present work is also favorably comparable with the values obtained from atomistic simulations of selfmated H-passivated a-C:H contacts (between 50 and 100 MPa), <sup>68,69</sup> which suggests that the macroscale response of the sliding contact is determined by the shear response of colliding nanoscale asperities.

However, the interfacial shear strength values computed from the experiments carried out with a-C:Gd $_{2.3~at.\%}$  and a-C:Eu $_{2.4~at.\%}$  films are significantly lower than those obtained in experiments performed with a-C films and approach the values measured for hydrogenated amorphous carbon under the most environmentally favorable conditions, namely inert or dry environments. As an example, Scharf et al. reported an interfacial shear strength of 9 MPa for diamond-like nanocomposite sliding against silicon nitride in dry nitrogen, 33 while Koshigan obtained an interfacial shear strength of  $(11 \pm 4)$  MPa in dry nitrogen and  $(13 \pm 5)$  MPa in dry air for hydrogenated amorphous carbon ([H] =  $(34 \pm 1)$  at.%)) containing silicon and oxygen ([Si] =  $(6 \pm 1)$  at.%; [O] =  $(3 \pm 1)$  at.%) sliding against 52100 steel.

Near-edge X-ray absorption fine structure (NEXAFS) spectromicroscopy measurements were performed to gain insights into the near-surface processes occurring on a-C, a-C:Gd<sub>2.3 at.%</sub>, and a-C:Eu<sub>2.4 at.%</sub> films upon sliding. Figure 3a

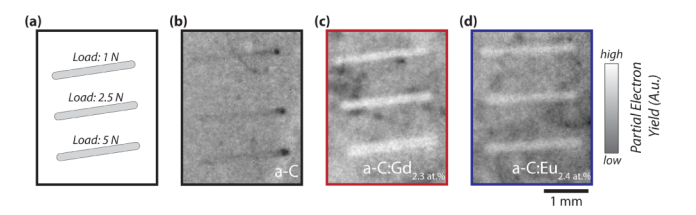


Figure 3. (a) Schematic of a typical specimen made of silicon wafer and coated with amorphous carbon films (a-C, a-C:Gd $_{2.3}$  at.%, or a-C:Eu $_{2.4}$ ). Three wear tracks were generated upon sliding a 52100 steel sphere at different applied normal load (1, 2.5, and 5 N); (b)–(d) partial electron yield NEXAFS maps acquired at a photon energy of ((285.0  $\pm$  0.2) eV) on a-C (b), a-C:Gd $_{2.3}$  at.% (c), and a-C:Eu $_{2.4}$  at.% films on which three tribological tests were performed at different applied normal load (1, 2.5, and 5 N).

shows a schematic of a typical specimen on which multiple tribological tests were performed at different applied normal loads. Owing to the large field of view (i.e., 13 mm × 18 mm) of the LARIAT full-field spectromicroscope,  $^{51,52}$  different wear tracks on a single specimen could simultaneously be imaged during the acquisition of NEXAFS image stacks, i.e., NEXAFS images collected while scanning the X-ray photon energy across the absorption edge of interest (e.g., carbon K-edge). Figure 3b–d display examples of NEXAFS C K-edge maps acquired in partial electron yield mode at a photon energy of (285.0  $\pm$  0.2) eV, which corresponds to the C 1s  $\rightarrow$   $\pi^*$  transition for sp² carbon–carbon (disordered) bonds.  $^{55,71}$  These maps enable the identification of the wear tracks and the extraction of NEXAFS spectra from regions of interest (ROIs), namely the contact (i.e., wear tracks) and non-contact regions.

Figure 4 displays pre- and post-edge normalized carbon K-edge spectra extracted from the contact and non-contact regions of a-C, a-C:Gd<sub>2.3 at.%</sub>, and a-C:Eu<sub>2.4 at.%</sub> films (a zoomed-in view of the absorption edge is provided on the graphs on the right-hand side). The spectra are characterized by a broad envelope between 287 and 320 eV originating from the C 1s  $\rightarrow \sigma^*$  transition for C–C  $\sigma$  (disordered) bonds. S5,71 Well-defined absorption features were detected at (285.0  $\pm$  0.2) eV, which corresponds to the C 1s  $\rightarrow \pi^*$  transition for

C=C  $\pi$  (disordered) bonds, <sup>55,71</sup> and at (288.9  $\pm$  0.2) eV, which corresponds to the C 1s o  $\sigma^*$  transitions for carbonoxygen bonds. 72,73 The presence of carbonyl groups in the probed volume slightly contributed to the spectral intensity between 286.5 and 287.0 eV (due to the C 1s  $\rightarrow \pi^*$  transition of C=O). 55,74 Finally, a weak absorption feature was detected at (287.0  $\pm$  0.2) eV and originated from the C 1s  $\rightarrow \sigma^*$ transition for C-H bonds. 55,75,76 Compared to the carbon Kedge NEXAFS spectrum extracted from the non-contact region of a-C the spectra obtained from the non-contact regions of a- $C{:}Gd_{2.3~at.\%}$  and a-C:Eu\_{2.4~at.\%} are characterized by a more intense feature assigned to the C 1s  $\rightarrow$   $\sigma^*$  transitions for carbon-oxygen bonds (at (288.9  $\pm$  0.2) eV). However, while in the case of a-C, no significant differences were observed between the spectra extracted from the wear tracks and the spectrum from the non-contact region, in the case of a- $C{:}Gd_{2.3~at.\%}$  and a-C:Eu<sub>2.4 at.\%</sub> films the carbon K-edge spectra obtained from the worn regions exhibited a reduced intensity of the absorption peak at  $(288.9 \pm 0.2)$  eV together with a slight increase in the feature at  $(285.0 \pm 0.2)$  eV. The former variation in spectral intensity can be ascribed to the removal of oxygen-containing surface terminating species, while the latter change in spectral intensity indicates the shear-induced rehybridization (from sp<sup>3</sup> to sp<sup>2</sup> bonding) of carbon atoms in the probed volume.

Finally, it has to be highlighted that independently of the film considered, compared to the spectra extracted from the non-contact region, the absorption feature assigned to the C 1s  $\rightarrow \pi^*$  transition for C=C (disordered) bonds<sup>55,71</sup> did not shift in photon energy, which indicates that, under the conditions used in the tribological tests carried out in the present work, no changes in the degree of ordering of the sp<sup>2</sup> C=C bonds occurred.<sup>55,71</sup>

The NEXAFS C K-edge spectra allowed the fraction of sp<sup>2</sup>bonded carbon atoms in the near-surface region of the amorphous carbon films to be determined (eq 1).53,71,75,76 Figure 5a displays the computed sp<sup>2</sup> carbon content as a function of the applied normal load used in tribological experiments, while Figure 5b shows the change in sp<sup>2</sup>-bonded carbon relative to the non-contact region as a function of the applied normal load. In the case of a-C films, the results obtained inside or outside the wear tracks were within the uncertainty of the measurements (e.g., the sp<sup>2</sup> carbon content was  $(43.8 \pm 0.9)\%$  in the non-contact region). In the case of the a-C films containing Gd or Eu, the fraction of sp<sup>2</sup>-bonded carbon in the non-contact region ((37.1  $\pm$  0.9) % for a-C:Gd<sub>2.3 at.%</sub> and (41.0  $\pm$  0.9) % for a-C:Eu<sub>2.4 at.%</sub>) was lower than the one in undoped a-C and increased upon increasing the applied normal load in the tribological experiments.

Altogether, the NEXAFS results indicated that the introduction of Gd and Eu into the a-C matrix increases the fraction of sp³-bonded carbon atoms in the as-deposited films. The stabilizing effect of Gd and Eu on sp³-hybridized carbon in a-C is postulated to be due to the reduction of residual stresses in the films induced by the introduction of these alloying elements in the a-C matrix, in a similar manner of the effect of incorporating metals into DLC coatings reported in the literature.<sup>32</sup> Furthermore, the imaging NEXAFS results indicated that no stress-assisted rehybridization (from sp³ to sp² bonding) of carbon atoms was induced by the sliding process in the case of the undoped a-C film, which contrasts the stress-induced formation of a lubricious a-C surface layer with a higher fraction of sp²-bonded carbon atoms in the case

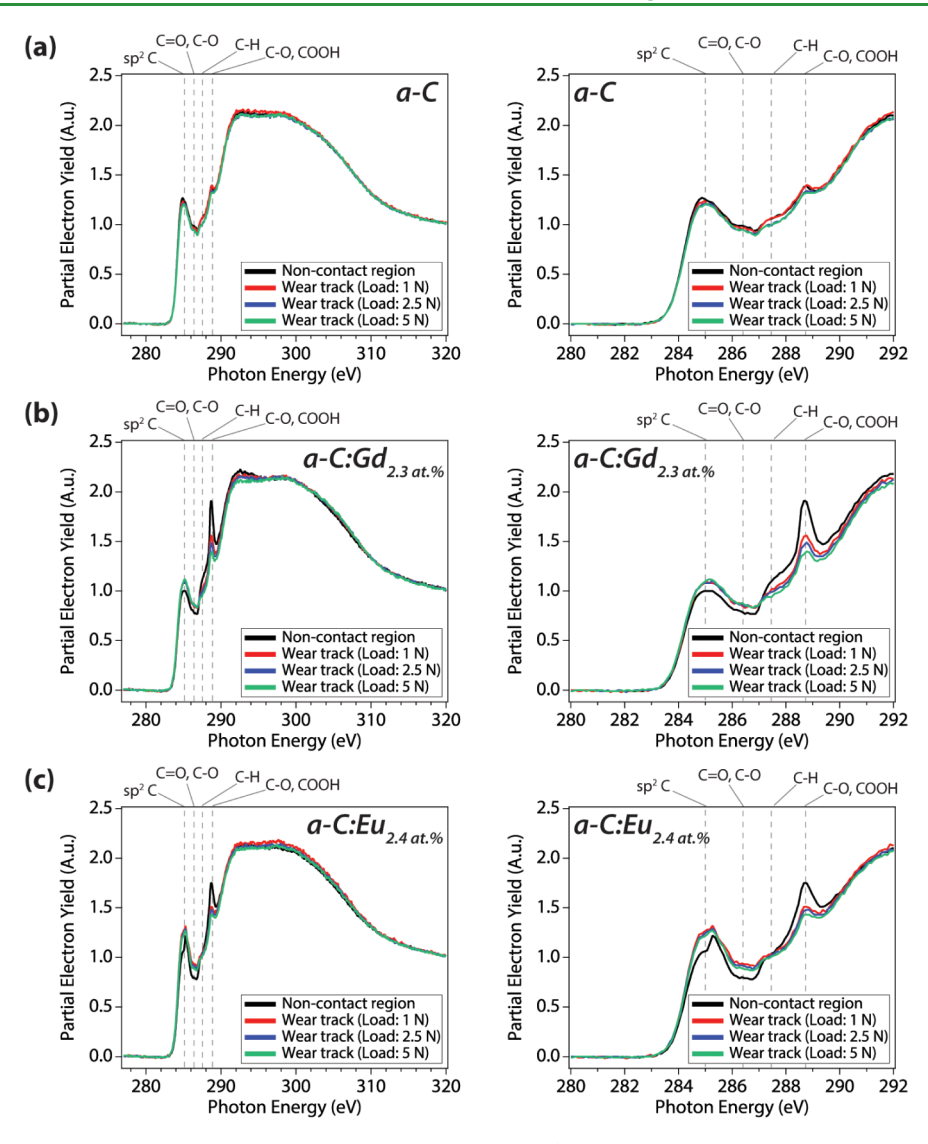
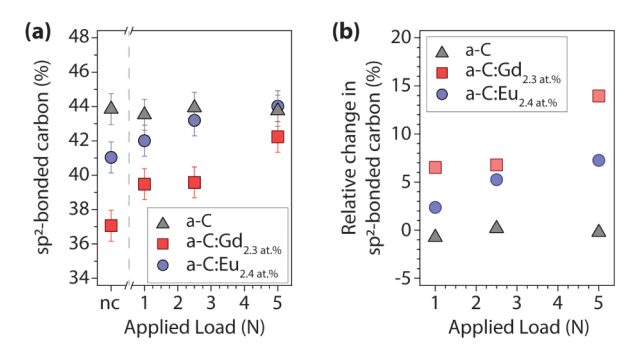


Figure 4. Partial electron yield C K-edge spectra extracted from regions of interest (non-contact region and wear tracks generated upon sliding at 1, 2.5, and 5 N applied normal load) of NEXAFS image stacks acquired on a-C (a), a-C:Gd<sub>2.3 at.%</sub> (b), and a-C:Eu<sub>2.4 at.%</sub> (c). Zoomed-in views of the spectra are displayed in the right column.



**Figure 5.** (a) Percentage of sp<sup>2</sup>-bonded carbon atoms in a-C, a-C:Gd $_{2.3}$  at $_{3.0}$ , and a-C:Eu $_{2.4}$  at $_{3.0}$  as a function of the applied normal load used in tribological tests. As a reference, the percentage of sp<sup>2</sup> carbon in the non-contact (nc) region is also reported. (b) Change in sp<sup>2</sup>-bonded carbon relative to the non-contact region in a-C, a-C:Gd $_{2.3}$  at $_{3.0}$ , and a-C:Eu $_{2.4}$  at $_{3.0}$  as a function of the normal load used in sliding tests.

of the a-C films alloyed with Gd or Eu. This preferential sp<sup>3</sup>-to-sp<sup>2</sup> rehybridization occurring in Eu- and Gd-containing a-C

coatings is attributed to the lower mechanical properties of these materials compared to the behavior of undoped a-C: the significant increase in Eu and Gd content in the outermost regions of the coatings (see XPS results shown in Figure S1) results in a drastic reduction of the surface mechanical properties, which promotes shear-induced plasticity in the coating and triggers the sp³-to-sp² rehybridization of carbon atoms in the a-C matrix. Conversely, the high shear-resistance of the undoped a-C film evaluated in the present study inhibits shear-induced plastic deformations and a significant change in the bonding configuration of carbon atoms from sp³ to sp².

Since Kuwahara et al.<sup>77</sup> recently provided evidence that, in the case of silicon-based ceramics sliding against a-C:H, the occurrence of plastic shear deformations (with sp³-bonded carbon atoms rehybridizing to sp² bonding) localized within the a-C:H coating is a necessary condition for the formation of a transfer film onto the countersurface, the contrasting shear behavior of doped and undoped a-C films detected in the present work suggests a completely different probability for the formation of a transfer film from these coatings to the steel countersurface. In other words, as the transfer-film process

preferentially occurs once a weak shear interface is created within a-C materials, the generation of a transfer layer on the steel countersurface should be more likely in the case of the experiments performed with Eu- and Gd-containing a-C films. To test this hypothesis, scanning electron microscopy (SEM) and energy-dispersive spectroscopy (EDS) measurements were carried out on the 52100 steel countersurfaces used in the tribological experiments.

Figure 6 displays both the secondary electron SEM micrographs (left column) and carbon EDS maps (right

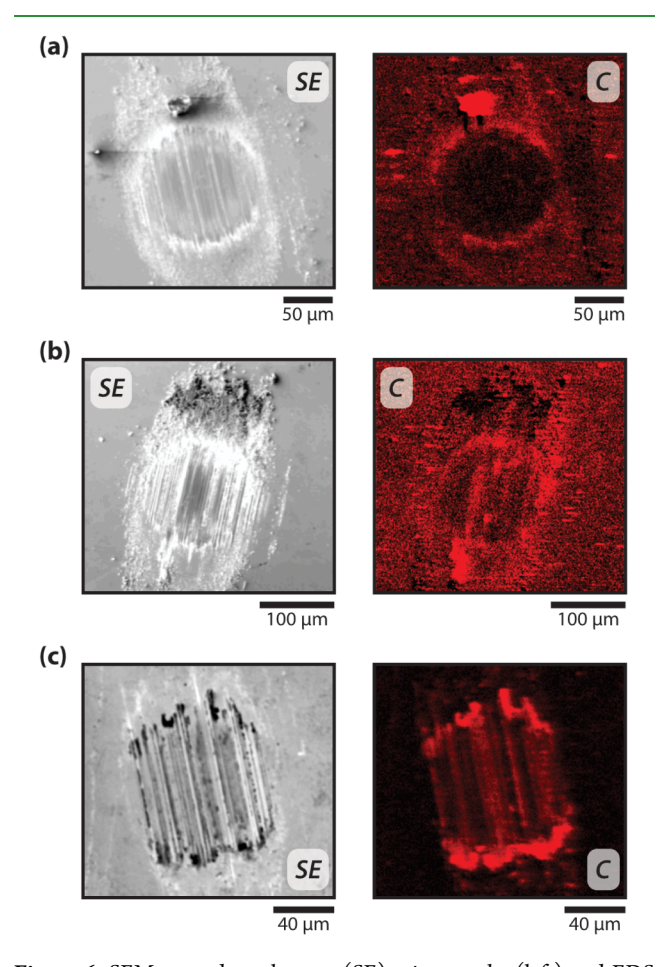


**Figure 6.** SEM secondary electron (SE) micrographs (left) and EDS carbon maps (right) acquired on 52100 steel spheres used in tribological experiments carried out on a-C (a), a-C: $Gd_{2.3 \text{ at.}\%}$  (b), and a-C: $Eu_{2.4 \text{ at.}\%}$  (c) at an applied load of 5 N.

column) acquired on spheres used in sliding tests performed at an applied normal load of 5 N. Upon examination of the countersurface employed in experiments with the a-C film, there was no transfer film present, and only a small amount of wear debris was found outside the contact region. In contrast, a carbonaceous transfer film was generated within the contact region in the case of the spheres that slid on a-C:Gd $_{2.3~at,\%}$  or a-C:Eu $_{2.4~at,\%}$  with a relatively large amount of loose, carbon-rich debris detected outside the contact region. This finding validates our hypothesis, while also substantiating the correlation between transfer-film process and formation of low shear-strength interfaces within a-C coatings reported by Kuwahara et al.

Altogether, the results presented in this study indicate that the introduction of Eu or Gd in a-C films deposited by HiPIMS results in the formation of an extended surface region with reduced mechanical properties, which facilitates shear-induced plasticity within the coatings and triggers the rehybridization of carbon atoms from sp³ to sp² bonding. The localization of shear deformations within the a-C layer and the stress-assisted sp³-to-sp² rehybridization of carbon atoms in Eu- or Gd-containing a-C films promote the transfer of materials to the sliding countersurface, thus significantly decreasing the interfacial shear strength.

The measured decrease in interfacial shear strength upon introducing Eu an Gd into the a-C matrix addresses a significant shortcoming of hydrogen-free a-C (also referred to as ta-C) thin films when used as a solid lubricating material in ambient conditions. Even though the friction response of ta-C films under humid conditions is significantly lower than the one under vacuum or inert environments,  $^{13-30}$  the measured coefficient of friction values are still quite high (0.1-0.2 against) different countersurface materials)  $^{62}$  compared to the other solid lubricants. For example, a-C:H might exhibit a lower friction coefficient (as low as 0.02)  $^{62}$  at high relative humidity values.

While the results of the present study can open the path for the potential use of a-C:Eu and a-C:Gd in specialized tribological applications requiring a low friction response under critical conditions for ta-C (i.e., humid air), the long-term use of Eu and Gd as alloying elements for a-C films might not be sustainable because of environmental and socio-economic reasons related to the employment of rare-earth elements. However, the outcomes of this work, providing insights into the mechanism with which soft alloying elements in a-C films contribute to reducing friction, provide guidelines for the rational design of lubricious DLC films alloyed with soft, non-rare-earth elements suitable for a variety of applications, such as coatings for micro- and nanoelectromechanical systems, high performance tools, hard disks, and atomic force microscope (AFM) probes.

## 4. CONCLUSIONS

In this work, the normal-pressure-dependent friction response of Eu- and Gd-containing a-C films deposited by HiPIMS on silicon was evaluated in open air and at room temperature. While the introduction of Eu and Gd ((2.4  $\pm$  0.1 at. %) and  $(2.3 \pm 0.1)$  at.%, respectively) into the a-C matrix resulted in a decrease in both elastic modulus and hardness as well as the presence of an extended near-surface layer with reduced nanomechanical properties compared to undoped a-C, the steady-state CoF for Eu- and Gd-containing a-C films was always lower than the one measured in the experiments carried out with a-C films. The results of normal pressure-dependent tribological experiments indicated a non-Amontonian friction behavior, i.e., a decrease in the coefficient of friction with the normal load, for all films deposited in the work and a significant reduction of the interfacial shear strength upon doping a-C films with Eu and Gd (computed interfacial shear strengths:  $(41 \pm 2)$  MPa for a-C,  $(16 \pm 1)$  MPa for a-C:Gd<sub>2.3 at.%</sub>, and (11  $\pm$  2) MPa for a-C:Eu<sub>2.4 at.%</sub>). NEXAFS spectromicroscopy experiments provided evidence that no stress-assisted rehybridization (from sp<sup>3</sup> to sp<sup>2</sup> bonding) of carbon atoms was induced by the sliding process in the nearsurface region of undoped a-C, while the amount of sp<sup>2</sup>bonded carbon in a-C:Gd<sub>2.3 at.%</sub> and a-C:Eu<sub>2.4 at.%</sub> progressively increased upon increasing the applied normal load in tribological tests. The formation of a sp<sup>2</sup>-bonded carbon-rich

a-C surface layer in a-C:Gd<sub>2.3</sub> at.% and a-C:Eu<sub>2.4</sub> at.% films is not only proposed to be the origin for the reduced duration of the running-in period in tribological tests carried out on these films (compared to the duration of the running-in in tests performed on undoped a-C), but also postulated to induce localized shear within the sp<sup>2</sup>-carbon rich layer and transfer film formation on the countersurface, thus decreasing the shear strength of the sliding interface. These findings open the path for the use of Gd- and Eu-containing a-C even under tribologically critical conditions for nearly hydrogen-free a-C films (i.e., humid air).

# ASSOCIATED CONTENT

# Supporting Information

The Supporting Information is available free of charge at https://pubs.acs.org/doi/10.1021/acsami.4c00677.

High-resolution XPS spectra acquired on as-deposited a-C, a-C:Gd<sub>2.3 at.%</sub>, and a-C:Eu<sub>2.4 at.%</sub>. (Figure S1); values of the fitting parameters, i.e., interfacial shear strength ( $\tau_0$ ) and pressure-dependent coefficient of the shear strength ( $\alpha$ ), obtained upon fitting the steady-state coefficient of friction as a function of the inverse Hertzian contact pressure (Table S1)(PDF)

## AUTHOR INFORMATION

## **Corresponding Author**

Filippo Mangolini — Walker Department of Mechanical Engineering, The University of Texas at Austin, Austin, Texas 78712, United States; Texas Materials Institute, The University of Texas at Austin, Austin, Texas 78712, United States; orcid.org/0000-0003-3360-9122; Email: filippo.mangolini@austin.utexas.edu

#### Authors

Camille Edwards – Walker Department of Mechanical Engineering, The University of Texas at Austin, Austin, Texas 78712, United States

Hsu-Ming Lien — Texas Materials Institute, The University of Texas at Austin, Austin, Texas 78712, United States; Materials Science and Engineering Program, The University of Texas at Austin, Austin, Texas 78712, United States; orcid.org/0000-0001-7262-9439

Nicolás Molina – Texas Materials Institute, The University of Texas at Austin, Austin, Texas 78712, United States; Materials Science and Engineering Program, The University of Texas at Austin, Austin, Texas 78712, United States

Complete contact information is available at: https://pubs.acs.org/10.1021/acsami.4c00677

## **Author Contributions**

C.E. contributed to investigation, data curation, formal analysis, and writing—review and editing; H.L. contributed to investigation, data curation, and writing—review and editing; N.M. contributed to investigation, data curation, and writing—review and editing; F.M. contributed to conceptualization, investigation, formal analysis, writing—original draft, funding acquisition, and writing—review and editing.

#### Notes

The authors declare no competing financial interest.

## ACKNOWLEDGMENTS

The material is based upon work supported by the Welch Foundation (Grant No. F-2151-20230405), the National

Science Foundation Faculty Early Career Development Program (Grant No. 2042304), and the FCT (Fundação para a Ciência e Tecnologia) under the Lub-Energy project (UTAP-EXPL/NPN/0046/2021). The acquisition of the VersaProbe-IV XPS was supported by the National Science Foundation Major Research Instrumentation program (Grant No. 2117623). The authors would like to thank Dr. Fábio Ferreira (University of Coimbra) for providing the coated silicon wafers for the study and information about the film composition. The authors would like to thank Dr. D.A. Fischer and Dr. C. Jaye for their help with NEXAFS measurements at the National Synchrotron Light Source II. The research used resources of the National Synchrotron Light Source II, a US Department of Energy (DoE) Office of Science User Facility operated for the DoE Office of Science by Brookhaven National Laboratory under Contract No. DE-SC0012704.

## REFERENCES

- (1) Tribology of Diamond-Like Carbon Films, Donnet, C.; Erdemir, A., Eds.; Springer: New York, 2008.
- (2) Erdemir, A.; Donnet, C.; Tribology of Diamond, Diamond-Like Carbon, and Related Films. In *Modern Tribology Handbook*, Bhushan, B., Eds.; CRC Press: Boca Raton, 2001.
- (3) Holmberg, K.; Andersson, P.; Erdemir, A. Global energy consumption due to friction in passenger cars. *Tribol. Int.* **2012**, 47, 221–234.
- (4) Fontaine, J. Towards the use of diamond-like carbon solid lubricant coatings in vacuum and space environments. *Proc. Inst. Mech. Eng., Part J* **2008**, 222 (8), 1015–1029.
- (5) Heaney, P. J.; Sumant, A. V.; Torres, C. D.; Carpick, R. W.; Pfefferkorn, F. E. Diamond coatings for micro end mills: Enabling the dry machining of aluminum at the micro-scale. *Diamond Relat. Mater.* **2008**, *17* (3), 223–233.
- (6) Ferrari, A. C. Diamond-like carbon for magnetic storage disks. Surf. Coat. Technol. 2004, 180–181, 190–206.
- (7) Kim, K.-H.; Moldovan, N.; Ke, C.; Espinosa, H. D.; Xiao, X.; Carlisle, J. A.; Auciello, O. Novel Ultrananocrystalline Diamond Probes for High-Resolution Low-Wear Nanolithographic Techniques. *Small* **2005**, *1* (8–9), 866–874.
- (8) Mangolini, F.; Rose, F.; Hilbert, J.; Carpick, R. W. Thermally induced evolution of hydrogenated amorphous carbon. *Appl. Phys. Lett.* **2013**, *103* (16), 161605.
- (9) Robertson, J. Diamond-like amorphous carbon. *Mater. Sci. Eng.*, R **2002**, 37 (4–6), 129–281.
- (10) Li, H.; Xu, T.; Wang, C.; Chen, J.; Zhou, H.; Liu, H. Tribochemical effects on the friction and wear behaviors of diamond-like carbon film under high relative humidity condition. *Tribol. Lett.* **2005**, *19* (3), 231–238.
- (11) Kim, H. I.; Lince, J. R.; Eryilmaz, O. L.; Erdemir, A. Environmental effects on the friction of hydrogenated DLC films. *Tribol. Lett.* **2006**, *21* (1), 51–56.
- (12) Ohtake, N.; Hiratsuka, M.; Kanda, K.; Akasaka, H.; Tsujioka, M.; Hirakuri, K.; Hirata, A.; Ohana, T.; Inaba, H.; Kano, M.; et al. Properties and Classification of Diamond-Like Carbon Films. *Materials* **2021**, *14* (2), 315.
- (13) Andersson, J.; Erck, R. A.; Erdemir, A. Frictional behavior of diamondlike carbon films in vacuum and under varying water vapor pressure. *Surf. Coat. Technol.* **2003**, *163*–*164*, 535–540.
- (14) Gardos, M. N. Surface chemistry-controlled tribological behavior of silicon and diamond. *Tribol. Lett.* **1996**, 2 (2), 173–187.
- (15) Gardos, M. N. Tribological fundamentals of polycrystalline diamond films. Surf. Coat. Technol. 1999, 113 (3), 183–200.
- (16) Tzeng, Y. Very low friction for diamond sliding on diamond in water. Appl. Phys. Lett. 1993, 63 (26), 3586–3588.
- (17) Harrison, J. A.; Brenner, D. W. Simulated Tribochemistry: An Atomic-Scale View of the Wear of Diamond. *J. Am. Chem. Soc.* **1994**, *116* (23), 10399–10402.

- (18) Harrison, J. A.; White, C. T.; Colton, R. J.; Brenner, D. W. Investigation of the atomic-scale friction and energy dissipation in diamond using molecular dynamics. *Thin Solid Films* **1995**, 260 (2), 205–211.
- (19) Perry, M. D.; Harrison, J. A. Universal Aspects of the Atomic-Scale Friction of Diamond Surfaces. *J. Phys. Chem.* **1995**, 99 (24), 9960–9965.
- (20) Moras, G.; Pastewka, L.; Walter, M.; Schnagl, J.; Gumbsch, P.; Moseler, M. Progressive Shortening of sp-Hybridized Carbon Chains through Oxygen-Induced Cleavage. *J. Phys. Chem. C* **2011**, *115* (50), 24653–24661.
- (21) Moras, G.; Pastewka, L.; Gumbsch, P.; Moseler, M. Formation and Oxidation of Linear Carbon Chains and Their Role in the Wear of Carbon Materials. *Tribol. Lett.* **2011**, *44* (3), 355–365.
- (22) Qi, Y.; Konca, E.; Alpas, A. T. Atmospheric effects on the adhesion and friction between non-hydrogenated diamond-like carbon (DLC) coating and aluminum A first principles investigation. *Surf. Sci.* **2006**, *600* (15), 2955–2965.
- (23) Zilibotti, G.; Righi, M. C.; Ferrario, M. Ab initio study on the surface chemistry and nanotribological properties of passivated diamond surfaces. *Phys. Rev. B* **2009**, *79* (7), 075420.
- (24) Manelli, O.; Corni, S.; Righi, M. C. Water Adsorption on Native and Hydrogenated Diamond (001) Surfaces. *J. Phys. Chem. C* **2010**, *114* (15), 7045–7053.
- (25) De Barros Bouchet, M.-I.; Zilibotti, G.; Matta, C.; Righi, M. C.; Vandenbulcke, L.; Vacher, B.; Martin, J.-M. Friction of Diamond in the Presence of Water Vapor and Hydrogen Gas. Coupling Gas-Phase Lubrication and First-Principles Studies. *J. Phys. Chem. C* **2012**, *116* (12), 6966–6972.
- (26) Zilibotti, G.; Corni, S.; Righi, M. C. Formation energy of dangling bonds on hydrogenated diamond surfaces: A first-principles study. *Phys. Rev. B* **2012**, *85* (3), 033406.
- (27) Zilibotti, G.; Corni, S.; Righi, M. C. Load-Induced Confinement Activates Diamond Lubrication by Water. *Phys. Rev. Lett.* **2013**, *111* (14), 146101.
- (28) Righi, M. C.; Zilibotti, G.; Corni, S.; Ferrario, M.; Bertoni, C. M. First-Principle Molecular Dynamics of Sliding Diamond Surfaces: Tribochemical Reactions with Water and Load Effects. *J. Low Temp. Phys.* **2016**, *185*, 174–182.
- (29) Levita, G.; Kajita, S.; Righi, M. C. Water adsorption on diamond (111) surfaces: an ab initio study. *Carbon* **2018**, *127*, 533–540.
- (30) Konicek, A. R.; Grierson, D. S.; Gilbert, P. U. P. A.; Sawyer, W. G.; Sumant, A. V.; Carpick, R. W. Origin of Ultralow Friction and Wear in Ultrananocrystalline Diamond. *Phys. Rev. Lett.* **2008**, *100* (23), 235502.
- (31) Kunze, T.; Posselt, M.; Gemming, S.; Seifert, G.; Konicek, A. R.; Carpick, R. W.; Pastewka, L.; Moseler, M. Wear, Plasticity, and Rehybridization in Tetrahedral Amorphous Carbon. *Tribol. Lett.* **2014**, 53 (1), 119–126.
- (32) Sánchez-López, J. C.; Fernández, A. Doping and Alloying Effects on DLC Coatings. In *Tribology of Diamond-Like Carbon Films: Fundamentals and Applications*, Donnet, C.; Erdemir, A., Eds.; Springer, 2008, pp. 311338.
- (33) Scharf, T. W.; Ohlhausen, J. A.; Tallant, D. R.; Prasad, S. V. Mechanisms of friction in diamondlike nanocomposite coatings. *J. Appl. Phys.* **2007**, *101* (6), 063521.
- (34) Yang, W. J.; Choa, Y.-H.; Sekino, T.; Shim, K. B.; Niihara, K.; Auh, K. H. Thermal stability evaluation of diamond-like nanocomposite coatings. *Thin Solid Films* **2003**, 434 (1–2), 49–54.
- (35) Demichelis, F.; Pirri, C. F.; Tagliaferro, A. Influence of silicon on the physical properties of diamond-like films. *Mater. Sci. Eng.* **1992**, *11* (1–4), 313–316.
- (36) Mangolini, F.; Hilbert, J.; McClimon, J. B.; Lukes, J. R.; Carpick, R. W. Thermally Induced Structural Evolution of Siliconand Oxygen-Containing Hydrogenated Amorphous Carbon: A Combined Spectroscopic and Molecular Dynamics Simulation Investigation. *Langmuir* 2018, 34 (9), 2989–2995.

- (37) Hilbert, J.; Mangolini, F.; McClimon, J. B.; Lukes, J. R.; Carpick, R. W. Si doping enhances the thermal stability of diamond-like carbon through reductions in carbon-carbon bond length disorder. *Carbon* **2018**, *131*, 72–78.
- (38) Mangolini, F.; Krick, B. A.; Jacobs, T. D. B.; Khanal, S. R.; Streller, F.; McClimon, J. B.; Hilbert, J.; Prasad, S. V.; Scharf, T. W.; Ohlhausen, J. A.; et al. Effect of silicon and oxygen dopants on the stability of hydrogenated amorphous carbon under harsh environmental conditions. *Carbon* **2018**, *130*, 127–136.
- (39) Koshigan, K. D.; Mangolini, F.; McClimon, J. B.; Vacher, B.; Bec, S.; Carpick, R. W.; Fontaine, J. Understanding the hydrogen and oxygen gas pressure dependence of the tribological properties of silicon oxide—doped hydrogenated amorphous carbon coatings. *Carbon* **2015**, *93*, 851–860.
- (40) Mangolini, F.; Koshigan, K. D.; Van Benthem, M. H.; Ohlhausen, J. A.; McClimon, J. B.; Hilbert, J.; Fontaine, J.; Carpick, R. W. How Hydrogen and Oxygen Vapor Affect the Tribochemistry of Silicon- and Oxygen-Containing Hydrogenated Amorphous Carbon under Low-Friction Conditions: A Study Combining X-ray Absorption Spectromicroscopy and Data Science Methods. ACS Appl. Mater. Interfaces 2021, 13 (10), 12610–12621.
- (41) Shaikh, S.; Omiya, T.; Cavaleiro, A.; Vilhena, L.; Ramalho, A.; Ferreira, F. Impact of Temperature Variation on Friction Behaviour of Rare Earth-Doped Diamond-like Carbon Coatings with Ionic Liquid Lubricants. *Lubricants* **2023**, *11* (7), 302.
- (42) Omiya, T.; Fontes, M.; Vuchkov, T.; Cruz, S.; Cavaleiro, A.; Ferreira, F. Tribological Performance of Gd-DLC and Eu-DLC Coatings in the Presence of Synthetic Oils Containing Ionic Liquid Additives. *Tribol. Lett.* **2023**, *71* (2), 65.
- (43) Fontes, M. A.; Serra, R. G. H; Fernandes, F. D.; Cavaleiro Rodrigues de Carvalho, A. A.; Ferreira, F. E. S. Comparison of mechanical and tribological properties of diamond-like carbon coatings doped with Europium and Gadolinium produced by HiPIMS. *Proc. Inst. Mech. Eng., Part B* **2022**, *0*, 09544054221136528.
- (44) Meng, K.; Yu, L.; Jing, S.; Tan, X.; Chen, X.; Wang, G. Microstructures, mechanical properties and surface wettability of Ladoped diamond-like carbon films deposited by magnetron cosputtering. *J. Alloys Compd.* **2023**, *934*, 167860.
- (45) Sadeghi, M.; Omiya, T.; Fernandes, F.; Vilhena, L.; Ramalho, A.; Ferreira, F. Tribological Behavior of Doped DLC Coatings in the Presence of Ionic Liquid Additive under Different Lubrication Regimes. *Coatings* **2023**, *13* (5), 891.
- (46) Zhang, L.; Lv, P.; Huang, Z. Y.; Lin, S. P.; Chen, D. H.; Pan, S. R.; Chen, M. Blood compatibility of La2O3 doped diamond-like carbon films. *Diamond Relat. Mater.* **2008**, *17* (11), 1922–1926.
- (47) Zhang, Z.; Lu, X.; Guo, D.; Xu, J.; Luo, J. Microstructure and mechanical properties of CeO2 doped diamond-like carbon films. *Diamond Relat. Mater.* **2008**, *17* (3), 396–404.
- (48) Li, Z.; Mangolini, F. Recent Advances in Nanotribology of Ionic Liquids. *Exp. Mech.* **2021**, *61* (7), 1093–1107.
- (49) Zhou, Y.; Qu, J. Ionic Liquids as Lubricant Additives: A Review. ACS Appl. Mater. Interfaces 2017, 9 (4), 3209–3222.
- (50) Oliver, W. C.; Pharr, G. M. Measurement of Thin Film Mechanical Properties Using Nanoindentation. *MRS Bull.* **1992**, *17* (7), 28–33.
- (51) Konicek, A.; Jaye, C.; Hamilton, M.; Sawyer, W.; Fischer, D.; Carpick, R. Near-Edge X-ray Absorption Fine Structure Imaging of Spherical and Flat Counterfaces of Ultrananocrystalline Diamond Tribological Contacts: A Correlation of Surface Chemistry and Friction. *Tribol. Lett.* **2011**, *44* (1), 99–106.
- (52) Mangolini, F.; McClimon, J. B.; Near Edge X-Ray Absorption Fine Structure Spectroscopy: A Powerful Tool for Investigating the Surface Structure and Chemistry of Solid Lubricants. In *Advanced Analytical Methods in Tribology*, Dienwiebel, M.; De Barros Bouchet, M. I., Eds.; Springer, pp. 63106, 2018.
- (53) Mangolini, F.; McClimon, J. B.; Carpick, R. W. Quantitative Evaluation of the Carbon Hybridization State by Near Edge X-ray Absorption Fine Structure Spectroscopy. *Anal. Chem.* **2016**, 88 (5), 2817–2824.

- (54) Mangolini, F.; Li, Z.; Marcus, M. A.; Schneider, R.; Dienwiebel, M. Quantification of the carbon bonding state in amorphous carbon materials: A comparison between EELS and NEXAFS measurements. *Carbon* **2021**, *173*, 557–564.
- (55) Stöhr, J.; Springer Series in Surface Sciences. In *NEXAFS Spectroscopy*; Springer-Verlag: Berlin Heidelberg, Vol. 25, 1992.
- (56) Mangolini, F. Reactivity of Environmentally Compatible Lubricant Additives: An in Situ and Ex Situ Investigation; ETH Zurich, 2011.
- (57) Mangolini, F.; Rossi, A.; Spencer, N. D. Chemical Reactivity of Triphenyl Phosphorothionate (TPPT) with Iron: An ATR/FT-IR and XPS Investigation. *J. Phys. Chem. C* **2011**, *115* (4), 1339–1354.
- (58) Bec, S.; Tonck, A.; Fontaine, J. Nanoindentation and nanofriction on DLC films. *Philos. Mag.* **2006**, *86* (33–35), 5465–5476.
- (59) Santra, T. S.; Liu, C. H.; Bhattacharyya, T. K.; Patel, P.; Barik, T. K. Characterization of diamond-like nanocomposite thin films grown by plasma enhanced chemical vapor deposition. *J. Appl. Phys.* **2010**, *107* (12), 124320.
- (60) Tillmann, W.; Lopes Dias, N. F.; Stangier, D.; Berndt, J.; Klemme, S.; Kesper, L.; Berges, U.; Westphal, C.; Thomann, C. A.; Debus, J. Rare-earth modified amorphous carbon films: Effects of erbium and gadolinium on the structural evolution and mechanical properties. *Diamond Relat. Mater.* **2022**, *123*, 108898.
- (61) Blau, P. J. On the nature of running-in. *Tribol. Int.* **2005**, 38 (11–12), 1007–1012.
- (62) Ronkainen, H.; Holmberg, K.; Tribology of Diamond-Like Carbon Films: Fundamentals and Applications. In *Environmental and Thermal Effects on the Tribological Performance of DLC Coatings*, Donnet, C.; Erdemir, A. Eds.; Springer US: Boston, MA, 2008; pp. 155200
- (63) Singer, I. L.; Dvorak, S. D.; Wahl, K. J.; Scharf, T. W. Role of third bodies in friction and wear of protective coatings. *J. Vac. Sci. Technol., A* **2003**, 21 (5), S232–S40.
- (64) Scharf, T. W.; Prasad, S. V. Solid lubricants: A review. *J. Mater. Sci.* **2013**, 48 (2), 511–531.
- (65) Scharf, T. W.; Singer, I. L. Role of Third Bodies in Friction Behavior of Diamond-like Nanocomposite Coatings Studied by In Situ Tribometry. *Tribol. Trans.* **2002**, 45 (3), 363–371.
- (66) Scharf, T.; Prasad, S.; Dugger, M.; Kotula, P.; Goeke, R.; Grubbs, R. Growth, structure, and tribological behavior of atomic layer-deposited tungsten disulphide solid lubricant coatings with applications to MEMS. *Acta Mater.* **2006**, *54* (18), 4731–4743.
- (67) Johnson, K. L.; Contact Mechanics; Cambridge University Press: Cambridge, 1985.
- (68) Pastewka, L.; Moser, S.; Moseler, M. Atomistic Insights into the Running-in, Lubrication, and Failure of Hydrogenated Diamond-Like Carbon Coatings. *Tribol. Lett.* **2010**, 39 (1), 49–61.
- (69) Kuwahara, T.; Long, Y.; De Barros Bouchet, M.-I.; Martin, J. M.; Moras, G.; Moseler, M. Superlow Friction of a-C: H Coatings in Vacuum: Passivation Regimes and Structural Characterization of the Sliding Interfaces. *Coatings* **2021**, *11* (9), 1069.
- (70) Koshigan, K. D.; Understanding the effect of environment on the tribological behavior of thin carbon based solid lubricants. Ecole Centrale de Lyon; Doctor of Dcience, 2015.
- (71) Comelli, G.; Stöhr, J.; Robinson, C. J.; Jark, W. Structural studies of argon-sputtered amorphous carbon films by means of extended x-ray-absorption fine structure. *Phys. Rev. B* **1988**, *38* (11), 7511–7519.
- (72) Wada, A.; Ogaki, T.; Niibe, M.; Tagawa, M.; Saitoh, H.; Kanda, K.; Ito, H. Local structural analysis of a-SiCx: H films formed by decomposition of tetramethylsilane in microwave discharge flow of Ar. *Diamond Relat. Mater.* **2011**, *20* (3), 364–367.
- (73) Ishii, I.; Hitchcock, A. P. The oscillator strengths for C1s and O1s excitation of some saturated and unsaturated organic alcohols, acids and esters. *J. Electron Spectrosc. Relat. Phenom.* **1988**, 46 (1), 55–84.
- (74) Osswald, S.; Yushin, G.; Mochalin, V.; Kucheyev, S. O.; Gogotsi, Y. Control of sp<sup>2</sup>/sp<sup>3</sup> Carbon Ratio and Surface Chemistry

- of Nanodiamond Powders by Selective Oxidation in Air. *J. Am. Chem. Soc.* **2006**, *128* (35), 11635–11642.
- (75) Sumant, A. V.; Gilbert, P. U. P. A.; Grierson, D. S.; Konicek, A. R.; Abrecht, M.; Butler, J. E.; Feygelson, T.; Rotter, S. S.; Carpick, R. W. Surface composition, bonding, and morphology in the nucleation and growth of ultra-thin, high quality nanocrystalline diamond films. *Diamond Relat. Mater.* **2007**, *16* (4–7), 718–724.
- (76) Mangolini, F.; McClimon, J. B.; Rose, F.; Carpick, R. W. Accounting for nanometer-thick adventitious carbon contamination in X-ray absorption spectra of carbon-based materials. *Anal. Chem.* **2014**, 86 (24), 12258–12265.
- (77) Kuwahara, T.; Long, Y.; Sayilan, A.; Reichenbach, T.; Martin, J. M.; De Barros Bouchet, M. I.; Moseler, M.; Moras, G. Superlubricity of Silicon-Based Ceramics Sliding against Hydrogenated Amorphous Carbon in Ultrahigh Vacuum: Mechanisms of Transfer Film Formation. ACS Appl. Mater. Interfaces 2024, 16, 8032–8044.